Development of a high performance surface slope measuring system for two-dimensional mapping of x-ray optics

Ian Lacey, Jérôme Adam, Gary Centers, Gevork Gevorkyan, Sergey Nikitin, et al.

Ian Lacey, Jérôme Adam, Gary P. Centers, Gevork S. Gevorkyan, Sergey M. Nikitin, Brian V. Smith, Valeriy V. Yashchuk, "Development of a high performance surface slope measuring system for two-dimensional mapping of x-ray optics," Proc. SPIE 10385, Advances in Metrology for X-Ray and EUV Optics VII, 103850G (7 September 2017); doi: 10.1117/12.2273029

SPIE.

Event: SPIE Optical Engineering + Applications, 2017, San Diego, California, United States

Development of a high performance surface slope measuring system for two-dimensional mapping of x-ray optics

Ian Lacey*[a], Jérôme Adam[a,b], Gary P. Centers[a,c], Gevork S. Gevorkyan[a], Sergey M. Nikitin[a], Brian V. Smith[a], and Valeriy V. Yashchuk[a]

[a]Lawrence Berkeley National Laboratory, 1 Cyclotron Rd., Berkeley, California 94720; [b]École nationale supérieure d'ingénieurs de Caen & Centre de Recherche (ENSICAEN), 6 Boulevard Maréchal Juin, 14000 Caen, France; [c]Helmholtz Institute, JGU Mainz, Staudingerweg 18, 55128 Mainz, Germany

ABSTRACT

The research and development work on the Advanced Light Source (ALS) upgrade to a diffraction limited storage ring light source, ALS-U, has brought to focus the need for near-perfect x-ray optics, capable of delivering light to experiments without significant degradation of brightness and coherence. The desired surface quality is characterized with residual (after subtraction of an ideal shape) surface slope and height errors of <50−100 nrad (rms) and <1−2 nm (rms), respectively. The ex-situ metrology that supports the optimal usage of the optics at the beamlines has to offer even higher measurement accuracy. At the ALS X-Ray Optics Laboratory, we are developing a new surface slope profiler, the Optical Surface Measuring System (OSMS), capable of two-dimensional (2D) surface-slope metrology at an absolute accuracy below the above optical specification. In this article we provide the results of comprehensive characterization of the key elements of the OSMS, a NOM-like high-precision granite gantry system with air-bearing translation and a custom-made precision air-bearing stage for tilting and flipping the surface under test. We show that the high performance of the gantry system allows implementing an original scanning mode for 2D mapping. We demonstrate the efficiency of the developed 2D mapping via comparison with 1D slope measurements performed with the same hyperbolic test mirror using the ALS developmental long trace profiler. The details of the OSMS design and the developed measuring techniques are also provided.

Keywords: 2-D surface slope map, NOM, error suppression, calibration, metrology of x-ray optics, surface metrology, nanoradian repeatability, synchrotron radiation

1. INTRODUCTION

The research and development work on the Advanced Light Source (ALS) upgrade to a diffraction limited storage ring (DLSR) light source, ALS-U,[1,2] has brought to focus the need for near-perfect x-ray optics, capable of delivering light to experiments without significant degradation of brightness and coherence. We need x-ray optics with surface quality characterized with residual (after subtraction of an ideal shape) surface slope and height errors of <50−100 nrad [root-mean-square (rms)] and <1−2 nm (rms), respectively. The x-ray optics of the same quality as that of the DLSR sources are required to entirely exploit the advantages of the fourth-generation synchrotron light sources and fully coherent free electron lasers (FELs).[3-7] The ex-situ metrology that supports the optimal usage of these optics at the beamlines must offer even higher measurement accuracy (see, for example, Ref.[8] and references therein).

At the ALS, the ex-situ metrology is concentrated in the X-ray Optics Metrology Laboratory (XROL).[9,10] Beginning 2014, the XROL has been in operation in a new laboratory space with comprehensive control of environmental conditions. This cleanroom facility is a factor of ~5 better than class 1000, with temperature stability better than ±30 mK over a day.[9,10]

The lab equipment includes a phase-shift interferometry microscope, a two-interferometer system (with capability for measurements of small radius of curvature, crucial for sagittally shaped x-ray mirrors), two slope-measuring long-trace profilers (upgraded LTP-II[11,12] and DLTP[13,14]), an atomic force microscope, optical microscopes, a differential laser Doppler vibrometer, and various systems for development of new x-ray optics and metrology techniques. With these instruments, the XROL delivers the state-of-the-art optical metrology required to build and maintain high performance

* ILacey@lbl.gov; phone 1 510 495-2159; fax 1 510 486-7696

Advances in Metrology for X-Ray and EUV Optics VII, edited by Lahsen Assoufid, Haruhiko Ohashi, Anand Krishna Asundi, Proc. of SPIE Vol. 10385, 103850G
 · doi: 10.1117/12.2273029

operations of the ALS beamlines.[15] For example, the upgraded LTP-II and DLTP are capable of one-dimensional surface slope profiling with the proven accuracy of tangential slope measurements with flat optics of ~60 nrad (rms) and accuracy with significantly curved optics (radius of curvature of ≥15 m) of ~200 nrad limited by the profiler's systematic errors.

Usage of different instruments ex situ enables us to separately investigate and address different potential sources affecting performance of optics at the ALS beamlines. These are surface quality (figure and finish errors), temporal and temperature dependence of surface shape, mechanical stability, gravity effect, alignments (twist, roll-off, yaw error), etc. All the perturbations at the beamline produce a cumulative effect to the performance of the optic that makes it difficult to optimize the optic's operational performance. The ex situ metrology allows us to fix a majority of problems before the installation of the optic at the beamline, and to provide feedback on design and guidelines on usage of optics (e.g., ambient temperature stability and accuracy of alignments).

The XROL actively participates in the research and development program associated with the ALS-U project. The major task for the lab is to develop optical metrology tools, measurement methods, and techniques adequate to its mission to assure the quality of the optical components mounted in a steerable support, installed in the ALS-U beamlines, and used as a part of the ALS-U experimental systems. This entails measuring mirrors to ensure vendor compliance to specifications, verifying that the quality of the optical surfaces is not degraded when the optics are assembled and cooled, as well as thorough mutual alignment of optical components, tuning, and characterization of the opto-mechanical systems.

To ensure the optimal usage of the super-high quality optics at the ALS-U, the dedicated ex situ metrology tools have to be capable for surface measurements with the accuracy better than the optical specification mentioned above by a factor of a few (2-5). Moreover, we need reliable and efficient surface metrology tools with a reasonably high measurement rate suitable for metrology with a large amount of optics coming for characterization, assembly, tuning, and alignment in the rather short period of time scheduled for installation of all the optics at ALS-U beamlines. The ex situ optical metrology used for assembling x-ray optical systems (e.g., end-station spectrometers and focusing KB mirror systems) and mutual alignment of their optical components have to be capable to measure with the required absolute accuracy of < 50 μm the relatively large multi-component systems, with characteristic sizes up to 2 meters. The range of tilt angles of the optical components is dictated by the grazing incidence angles characteristic for soft x-ray optics, and can reach a dozen degrees. The accuracy of measurement for the angular alignment has to be < 50 μrad.

The current performance of the optical metrology at the ALS XROL is close to the requirements for the ALS-U optics only for measurements with plane and relatively small optics. The accuracy achieved in measurements with significantly curved and sagittally shaped optics is worse by a factor of about 2-4 than the specification, as in the case of slope measurements. This reflects the general situation with ex situ metrology for x-ray optics. The metrology methods, approaches, and tools currently in use at the ALS XROL and other DOE BES light source facilities, as well as in the U.S.A. optical industry, including traditional long trace profilometry, deflectometry, and interferometry, have basically reached their limits. These limits are caused mostly by the level of inherent instrumental systematic errors and temporal instabilities, the low measurement rate, and an unacceptably high cost. Further improvement of the optical metrology requires a deep revision of the basic schematics and principles placed in the foundation of these instruments and implementation of innovative approaches, experimental techniques and methods under development around the word. It is for this reason that the XROL is a critical partner in the development of metrology for next-generation optics, and many R&D projects are underway in close collaboration with the x-ray optical teams at x-ray facilities in U.S.A. and around the world, as well as with the U.S.A. industry (see Refs.[16-22] and references therein).

Here, we report on our first results on the development at the ALS XROL of a new slope measuring profiler – the Optical Surface Measuring System (OSMS) – capable of absolute surface slope metrology of better than 50 nrad. This project is, in some sense, a continuation of the efforts of a broad collaboration including DOE x-ray facilities and vendors of x-ray optics with active participation of the HBZ/BESSY-II optics group[16] that formulated the major requirements to the design and performances of the OSMS gantry system. Based on the consideration in Ref.,[16] a high-performance gantry system for a new generation of optical slope measuring profilers has been developed at the Argonne Photon Source (APS).[17,23] In our case, we have adopted the design of the gantry system firstly developed for the HZB/BESSY-II nanometer optical measuring (NOM) surface slope profilometer.[24,25] A number of NOM-like system based on an electronic auto-collimator (AC) and a movable pentaprism are currently in use at the x-ray facilities around the world.[26-31] The distinguished feature of our gantry system (see Sec. 2) is the custom tilting and flipping stage that opens a new capabilities for development of a super high accuracy measuring system for two-dimensional (2D) surface

slope metrology with state-of-the art x-ray optics (Sec.3). In Sec. 4, we show that the gantry system supports the repeatability on the level below 20 μrad (root-mean-square, rms) in auto-collimator measurements with an x-ray hyperbolic cylinder mirror.

2. THE XROL OSMS GANTRY SYSTEM

The major XROL efforts on metrology instrumentation research and development are directed to creation of a new Optical Surface Measuring System capable of 2D surface-slope metrology at absolute accuracy below 50 nrad (in the slope domain) and < 1 nm (in the height domain). The OSMS granite gantry system consisting of a 2D air-bearing translation system and a precision air-bearing stage for tilting and flipping the surface under test (SUT) have been specified, purchased, installed, and commissioned at the XROL in 2015-2016 (Fig.1). Our next goal is to develop state-of-the-art optical sensors for the OSMS. The work is in progress at the XROL.

2.1 Design

The key element of the OSMS under development is its gantry system that, in our case, is better to call 'multifunctional translation system (MFTS) – Fig. 1a. The standard NOM-like gantry system[24,25] allows automatically controlled scanning of the sensor optical head across the SUT in two orthogonal directions. Scanning along the longitudinal *X*-direction is provided with translation of a carriage air-bearing suspended on a long beam of a bridge-type translation stage. By moving a base slab with large air-bearing surface across the base of the gantry system, the SUT can be translated along the sagittal *Y*-direction.

In addition to these two translations, the OSMS MFTS has a precise tilting/flipping stage capable for automatically controlled tilting and rotation of the SUT in the course of a measurement run, as well as vertical (*Z*-axis) shifting of the SUT. These additional translations are crucial for implementation of experimental methods to automatically suppress the errors in a measurement run via optimal arrangement of repeatable scans.[32-35]

The OSMS MFTS shown in Fig. 1a was custom designed and fabricated by Q-Sys Company.[36] All the motion controls and data acquisition systems are based on the NI LabView™ platform.

(a) 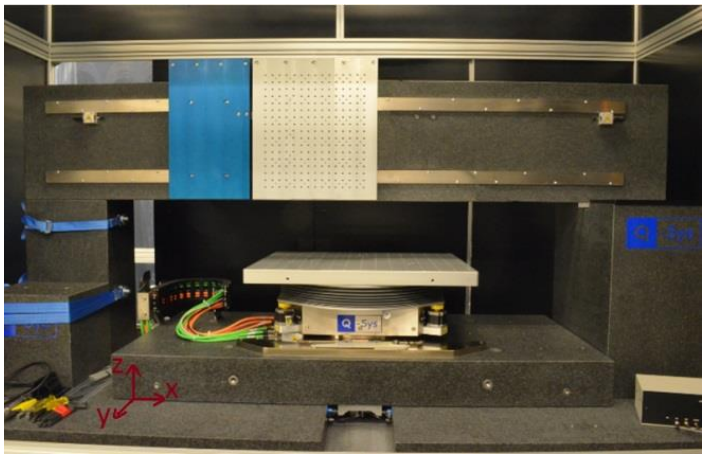 (b) 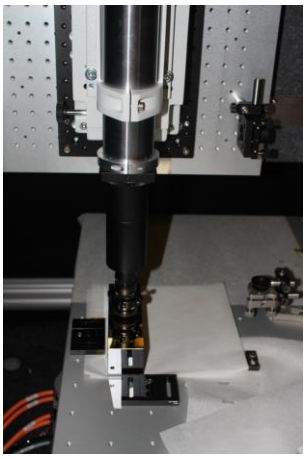

Figure 1: (a) The OSMS multifunctional translation system (MFTS) installed in the ALS XROL. (b) Experimental arrangement of measurements with a hyperbolic cylinder mirror with an autocollimator mounted on the OSMS MFTS carriage.

2.2 Performance of the MFTS spatial translations

The performance of the MFTS linear translations of the carriage and the granite slab were investigated via comparison of the displacement measured with the corresponding MFTS built-in linear encoders with the distance measured with the additional reference interferometers. As the references, we used an OPTODYNE displacement measuring interferometer (DMI)[37] and an Attocube integrated displacement sensing (IDS) interferometer.[38] Usage of two different reference interferometers allows us to separate the errors related to the translation stage from the systematic errors in the reference measurements.

2.2.1 *X*-axis translation

Figure 2 reproduces the results of tests of *X*-axis translation using the OPTODYNE DMI as a reference. The two traces of 1 meter length in Fig. 2 correspond to two runs, each of 4 scans (arranged to suppress a possible drift error described with the second order polinimial;[34] see also Sec. 3.1) of the carriage with simultaneous recording the translation distance with the built-in carriage linear encoder and the OPTODYNE DMI. The two traces were recorded with the opposite orientations of the DMI with respect to the OSMS scanning direction. Comparison of these two measurements allows us to conclude that the low spatial variation of the distance is due to the carriage translation, rather than to be a systematic error of the DMI.

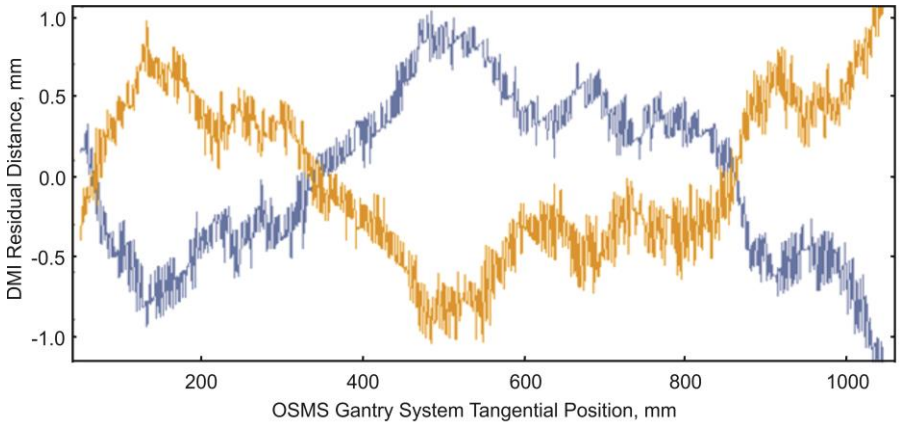

Figure 2: Residual (after subtraction the best fit linear dependence) *X*-distance variation of the four averaged scans as measured with the OPDYNE DMI on the two opposite sides.

Similar measurements as in Fig. 2, but performed with the Attocube IDS interferometer allows us to attribute the higher spatial frequency variation to the systematic error inherent to the OPTODYNE DMI. In the cross-comparison measurements with the two reference tools, we have also established a problem related to the linear calibration of the OPTODYNE DMI that found to be equal to 1.00345 mm/mm. This is probably due to the dependence of the calibration on the specific air pressure and humidity in the lab, different from the environment of the DMI when it was calibrated.

The final result for the positioning error of the *X*-translation of the OSSM gantry system is a 2 μm peak-to-valley and 0.5 μm rms variations. Note that due to the systematic character of the distance error, it can be easily accounted for in the data acquisition software. It is interesting to remark that for relatively short mirrors (SUTs) we can use X-scanning between ~ 150 mm and ~ 500 mm where the nonlinearity is minimum.

2.2.2 *Y*-axis translation

Figure 3 reproduces the results of tests of *Y*-axis translation using the OPTODYNE DMI as a reference.

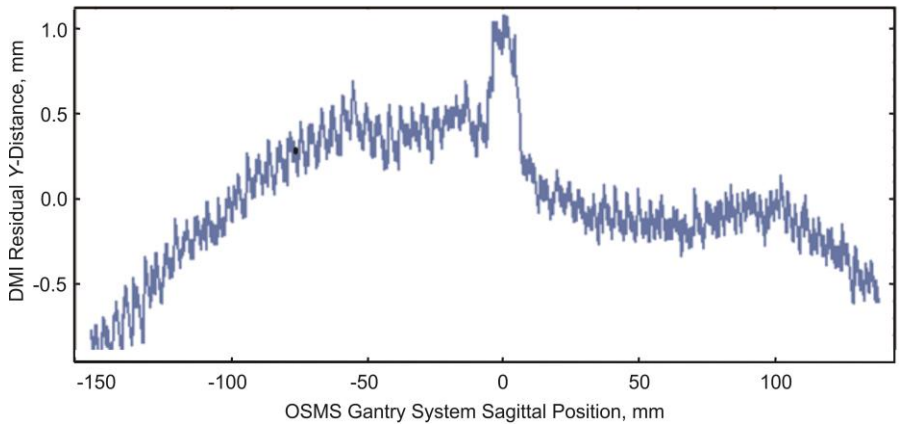

Figure 3: Residual (after subtraction the best fit linear dependence) *Y*-distance variation of the four averaged scans as measured with the OPDYNE DMI.

In this case the MFTS granite slab was translated by 300 mm (the entire range of the slab translation) with 0.2 mm increment and the translation distance were recorded with the corresponding linear encoder built in the MFTS.

For a better understanding of the origin of the error of *Y*-translation depicted in Fig. 3, the measurements were repeated with the DMI and its back-reflecting mirror switched in position on the granite base and *Y*-translational slab with each other. With the DMI and the mirror placed on either position, the residual distance variation errors of the *Y*-axis positioning appeared to be very similar. In addition to the small perturbations due to the DMI, a sharp perturbation of about 1 μm peak-to-valley (PV) was observed at the position of the index between approximately ±8 mm. This is neither due to random or drift errors because a mean of the four scans suppresses these errors, nor due to systematic errors of the DMI because the main shape appears at exactly the same position of the slab in either orientation. Thus this sharp perturbation, as well as the entire residual error in Fig. 3 belongs to the *Y*-coordinate gantry positioning system.

Over the entire range of 300 mm (Fig. 3), the final result for the positioning error of the *Y*-axis of the OSSM gantry system is a 2 μm PV and 0.38 μm rms variations.

2.2.3 *Z*-axis translation

The process of determining the accuracy of the Z-coordinate was made in a similar manner to the other two axes. In this case, the DMI was mounted on the carriage, while the corner cube reflector was attached to the stage's platform. The tilting/flipping stage can go up and down using the coordinated motion of the three motors, each having its own encoder to control the stage tilt. This allows for *Z*-axis translation of about 50 mm. To better understand the coordinated motion between the actuators, the measurements were performed at four different positions with the cube back-reflector placed above each of the three motors and in the center of the platform.

The major result of the measurements is that the translation is very linear and repeatable. However, the measurements reveal a significant linear calibration error of about 3.9% that has to be accounted in the motion control software.

3. TWO DIMENSIONAL MEASUREMENT WITH SUPPRESSION OF DRIFT ERROR

3.1 Optimal scanning strategy method and drift error suppression

The experimental method for effective suppression of spurious effects in slope measurements caused by slow instrumental drifts was suggested and first demonstrated in Ref.[34] According to the method, a slope trace measurement run consists of a number of repeatable scans arranged with a sequential reversal of the direction of scanning towards increasing (Forward) or decreasing (Backward) in x_i and/or the orientation of the SUT with respect to the slope profiler. Such a run provides repeatable measurements at a certain point x_i at a sequence of time moments $t_i(s)$, where s is the scan number ($s = 1, 2, ..., S$), specially arranged according to optimal scanning strategies analytically derived in Ref.[34] to anti-correlate with the temporal dependence of the drift.

Denoting the directionality of the s-th scan with r_s,

$$r_s = \begin{cases} \text{F} & \text{if the s-th scan is performed in the forward direction,} \\ \text{B} & \text{if the s-th scan is performed in the backward direction,} \end{cases} \quad (1)$$

optimal scanning strategies, suitable for suppression of a linear drift, are straightforward:

$$r_s(1) = \{F, B\} \quad \text{and} \quad r_s(1) = \{B, F\} \quad (2)$$

As shown in Ref.,[34] suppression of drifts of the second order would require a run consisting of 4 scans

$$r_s(2) = \{F, B, B, F\} \quad \text{or} \quad r_s(2) = \{B, F, F, B\}, \quad (3)$$

and for third order,

$$r_s(3) = \{F, B, B, F, B, F, F, B\} \quad \text{or} \quad r_s(3) = \{B, F, F, B, F, B, B, F\}, \quad (4)$$

Solutions (2-4) suggest that the suppression of any order drift automatically suppresses lower orders.

There is no apparent preferred directionality of the scans, so it is natural that if the set $\{r_s\}$ is a solution then the set $\{-r_s\}$ is also a solution [as depicted with Eqs. (2-4)]. Denoting the positive solution (started from the forward direction scan) for the p -th order drift suppression as $\left\{r_s^+(p)\right\}$ and the negative solution (started from the backward direction scan) as $\left\{r_s^-(p)\right\}$, the general recursion relation[34] between the sets $\left\{r_s^\pm(p+1)\right\}$ and $\left\{r_s^\pm(p)\right\}$ is

$$\left\{r_s^\pm(p+1)\right\} = \pm\left\{r_s^+(p), r_s^-(p)\right\}. \tag{5}$$

For the case when only the scanning direction is reversed, the corresponding suppression factor can be estimated[34] as a ratio of PV variations of the major terms of the drift error of the optimized and non-optimized runs of the same total number of scans:

$$\xi \cong 8 \cdot 2^p / p. \tag{6}$$

Estimation (6) shows that suppression factor, ξ, rapidly increases with increase of p for $p \geq 2$.

3.2 Extension of the optimal scanning strategy method to 2D slope measurements

In Ref.[39], in order to get a 2D slope topography of the SUT, a multiple 1D tangential traces are measured with a sequential translation of the SUT in the sagittal direction. In order to account for the drift error and misalignment of the mirror upon the sagittal shifts, additional sagittal and diagonal traces are used to reliably stitch the tangential traces. This significantly complicates and draws out the 2D data acquisition and data processing.

Extension of the optimal scanning strategy method suggested in this paper allows automatic suppression of drift error in the two-dimensional surface slope measurements with the 2D spatial translation of the OSMS MFTS (Sec. 2). In this case (see Fig. 4), a measurement run to collect a 2D slope map consists of a number of repeatable 2D scans in the forward (Fig. 4a) and the backward (Fig. 4b) direction, optimally arranged according to the prescription given in Sec. 3.1 with Eqs. (2-4).

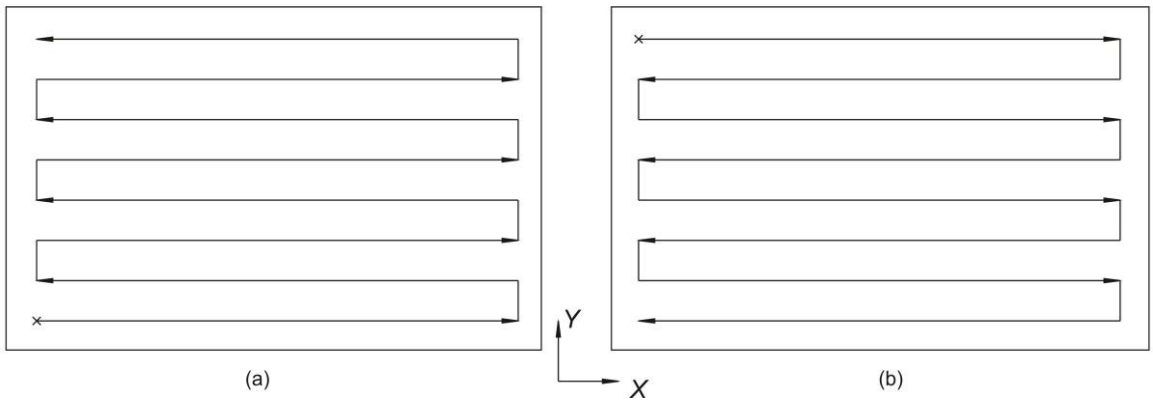

Figure 4: (a) 2D scan in the forward and (b) in the backward direction. The 2D scans starting from tracing in *X*-direction are shown. A similar definition of the forward and backward scans can be applied to 2D scans that start from the measurement in *Y*-direction. The crosses depict the starting points of the scans.

When the drift error is suppressed by application of the optimal scanning strategy method, the systematic error due to the mirror shifts (for example, in the sagittal direction, if the scans are performed according to the pattern depicted in Fig. 4) can be accounted via additional calibration of the wobbling effect of the translation stages.

4. 2D SLOPE MAPPING OF A HYPERBOLIC MIRROR WITH THE ALS OSMS EQUIPPED WITH AN AUTOCOLLIMATOR MOUNTED TO THE CARRIAGE

Figure 1b shows the experimental arrangement of the ALS OSMS equipped with an autocollimator directly mounted to the carriage in the vertical orientation. This arrangement was used for the measurements with a hyperbolic cylinder x-ray mirror developed for the ALS QERLIN beamline.[40] The goal of the measurements was to investigate the performance of

the OSMS gantry system in application to the 2D surface slope mapping. The major spurious effects expected are the AC systematic error and the pitch wobbling of the *X*- and *Y*-translations of the carriage and the slab, respectively. With the auto-collimator mounted directly to the carriage, the measurements are most sensitive to both wobbling effects.

4.1 Reference 1D slope measurements with the ALS DLTP

As the reference data, we used the results of 1D slope measurements with the same hyperbolic cylinder x-ray mirror performed using the ALS DLTP.[13,14]

The mirror substrate with overall dimensions of 160 × 50 × 50 mm^3 and clear aperture (CA) of 150 × 20 mm^2 are made of gold coated single crystal <100> silicon. The hyperbolic cylinder shape of the mirror is specified in the terms of the mirror beamline application (conjugate) parameters R_1, R_2, and θ, where R_1 and R_2 are focal radii and θ is the grazing incidence angle at the mirror center:

$$R_1 = 700\,\text{mm},\ R_2 = 1781.97\,\text{mm},\ \text{and}\ \theta = 2.0\,\text{degrees}; \tag{7}$$

here R_1 is the distance between the object to hyperbolic mirror center, whereas R_2 is the distance from the second (virtual) focus to the center of the hyperbolic mirror. The overall tangential slope variation is about 2 mrad. The surface slope error is specified to be < 250 nrad (rms) and < 3.0 µrad (rms) in the tangential and sagittal directions, respectively.

Figure 5 shows the residual (after subtraction of the desired hyperbolic shape) slope traces measured with a 0.2 mm increment along two tangential lines within the mirror clear aperture shifted from the center in the sagittal direction by ±5 mm, as specified for the mirror acceptance measurements. Each trace in Fig. 5 is the result of averaging over 4 runs of 8 scans arranged according to the scanning strategy given with Eq. 4, optimal to suppress the instrumental and set-up drifts described with the third order polynomial. The four runs include 2 pairs of runs with two different orientations (direct and flipped) of the mirror. The two runs measured at the same mirror orientation are different in the relative pitch tilt of 140 µrad, used in order to suppress the major known quasiperiodic (with a period of ~280 µrad) systematic error of the DLTP.[41] The rms variations are 168 nrad and 163 nrad for the top and bottom traces in Fig. 5, respectively.

Averaging of the runs with different mirror orientations allows additional suppression of the even part of the systematic slope error of slope measurements.[42] The suppressed even part of the error can be found as a half of the difference of the runs with different mirror orientations. In our case, the rms variations of the error even parts are 75 nrad and 78 nrad for the top and bottom traces in Fig. 5, respectively. Because absence of a better estimation of the residual odd part of the error contributed to the resulted traces in Fig. 5, we can only suppose that it has an rms variation close to that of the error even part, estimated to be ~80 nrad.

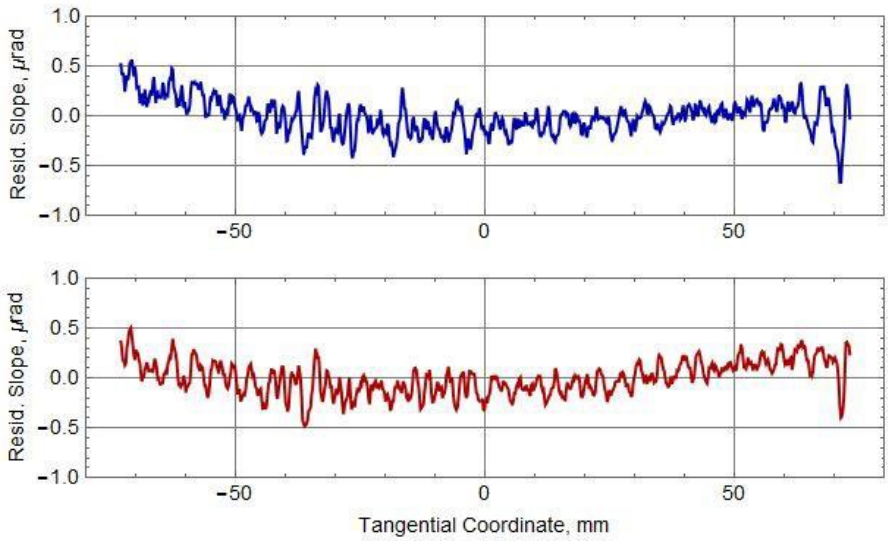

Figure 5: The residual (after subtraction of the desired hyperbolic shape) slope traces measured along two lines of the entire tangential length of the mirror clear aperture shifted from the center in the sagittal direction by ±5 mm, specified for the mirror acceptance measurements. The rms variations are 168 nrad and 163 nrad for the top and bottom traces, respectively.

4.2 Performance tests of the ALS OSMS MFTS

The OSMS measurements with the hyperbolic mirror were performed as 2D runs consisting of three tangential traces including two traces measured with the DLTP and an additional trace along the sagittal center of the mirror. Therefore, the increments are 0.2 mm and 5 mm for the tangential and sagittal directions, respectively. The total duration of one run consisted of 8 optimally arranged scans is 37 hours.

The results of two runs are discussed below. The first run was performed with the mirror oriented with the tangential axis along *X*-direction. In this case, scanning in the tangential direction was carried out with the carriage, whereas the shifting in the sagittal direction was made with the air-bearing slab. For the second run, the mirror was rotated by 90 degrees and scanning in the tangential direction was carried out with translation of the slab and the sagittal shifts with the carriage.

In the performed OSMS measurements (when we did not apply our methods for suppression of the systematic errors[35,41]) provided tangential traces that are compromised by the AC systematic error and the error related to the imperfection (pitch wobbling) of the OSMS carriage and slab. In order to illuminated the systematic error of the OSMS measurements, the tangential traces obtained with the OSMS were detrended with the corresponding surface slope variations measured with the DLTP.

Figures 6 and 7 depict the difference of the OSMS and DLTP traces measured by scanning along the mirror tangential direction the OSMS carriage (Fig. 6) and the air-bearing slab (Fig. 7). The slope difference traces can be thought of as the measures of the OSMS systematic errors for scanning in *X*- and *Y*-directions. In the figures, we also show the residual slope error traces that are the dissimilarity of the corresponding slope difference traces.

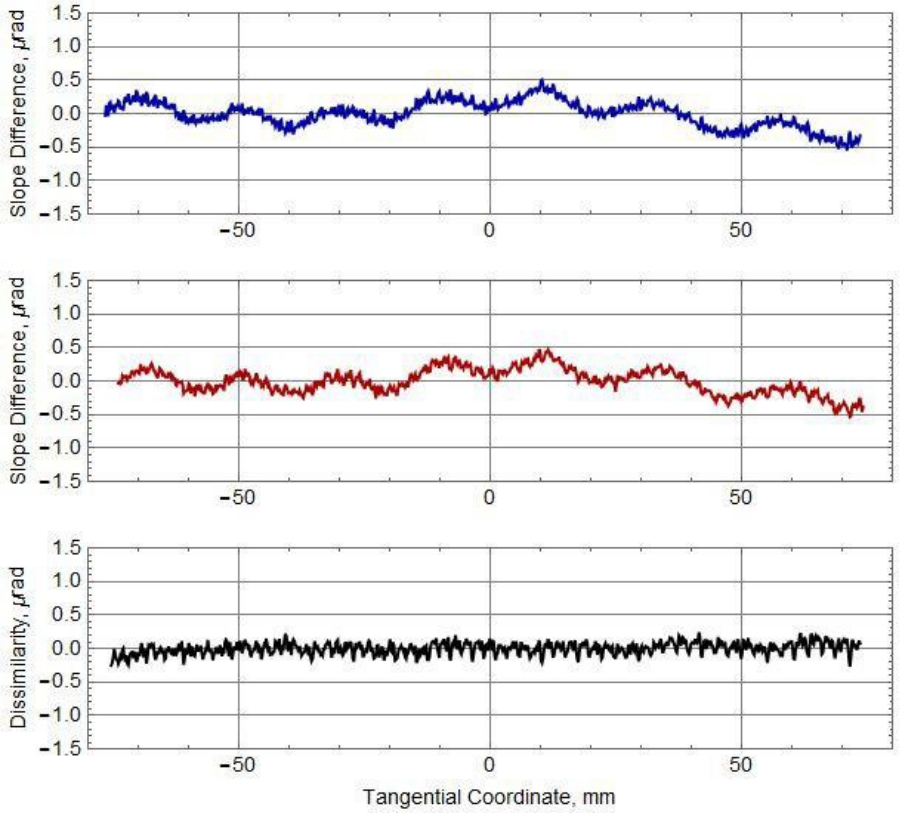

Figure 6: The systematic error of a single OSMS run with scanning the OSMS carriage along two 150-mm long traces within the clear aperture of the hyperbolic cylinder mirror (the two top traces). The systematic error was found as the difference of the corresponding OSMS and DLTP. (the bottom trace) The slope error dissimilarity trace depicting the difference of the two upper traces of the systematic error. The rms variations of the traces are 177 nrad, 176 nrad, and 88 nrad, from the top to bottom. The tilt of the upper traces can be characterized with an effective radii of a convex curvature of 544.3 km and 751.2 km.

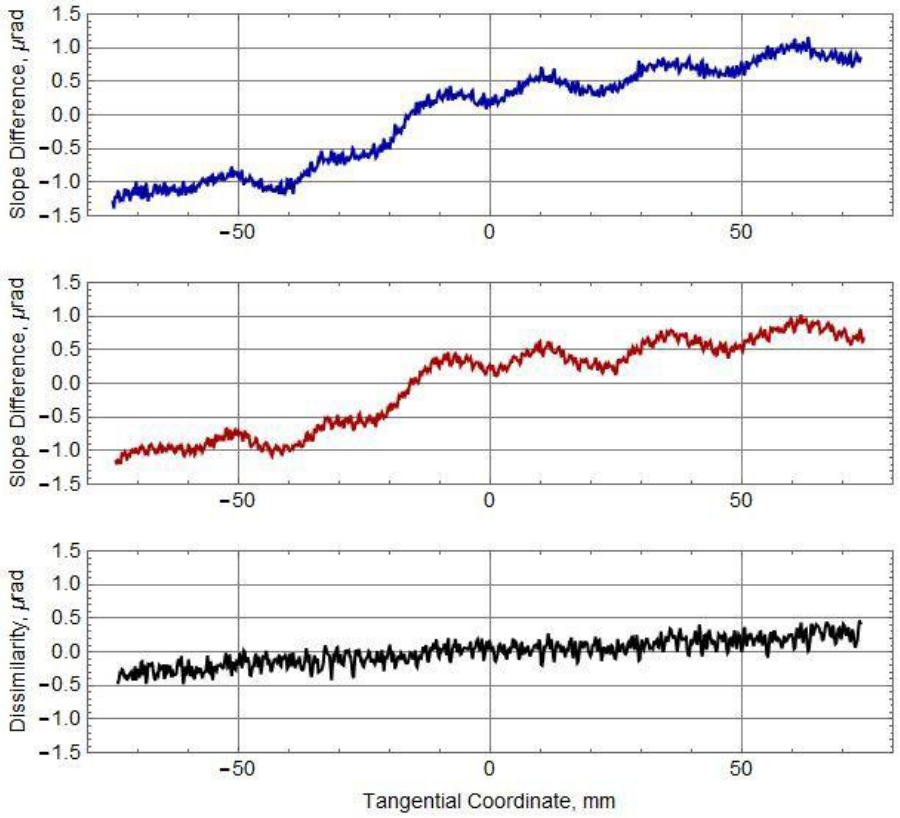

Figure 7: The systematic error of a single OSMS run with scanning the OSMS air-bearing slab along two 150-mm long traces within the clear aperture of the hyperbolic cylinder mirror (the two top traces). The systematic error was found as the difference of the corresponding OSMS and DLTP. (the bottom trace) The slope error dissimilarity trace depicting the difference of the two upper traces of the systematic error. The rms variations of the traces are 221 nrad, 223 nrad, and 100 nrad, from top to bottom. The tilt of the upper traces can be characterized with an effective radii of a concave curvature of 58.9 km and 67.5 km.

The most noticeable feature seen in the all systematic error traces in Figs. 6 and 7 is the quasiperiodic variations with the characteristic angular period of about 280 μrad. This systematic error is similar to the one that was suppressed in the DLTP measurements by tilting the mirror by 140 μrad (Sec. 4.1).

The slight common tilt of the systematic error traces probably reflects the corresponding wobbling errors of the gantry system that can be characterized with the effective radius of curvature of ~600 km and ~60 km for the carriage and slab translations. These contributions to the systematic error of the OSMS measurements can be effectively calibrated out with additional monitoring of the wobbling pitch angle variations. Note that in the traditional NOM arrangement with a stationary auto-collimator and movable pentaprism, the measurements are not sensitive to the small pitch wobbling of the carriage. In this case, one needs to monitor only the slab wobbling.

The high stability of the measurements can be seen from the dissimilarity traces that mostly contain the higher spatial frequency quasiperiodic variations with the characteristic angular periods of about 12 and 24 μrad. These are also the known quasiperiodic systematic errors of the OSMS auto-collimator.[41] This error also can be suppressed via averaging with an additional run performed with a tilt corresponding to a half of this period.

It is interesting to mention that the observed high angular frequency systematic error has survived upon averaging of 8 scans recorded in a 1.5-day-long non-stop run. This is due to the extremely high stability of the lab environmental conditions and the experimental arrangement, when the overall drift of the slope measurements is only about 1 μrad (PV). From the experimental point of view, it would be even more beneficial if the drift is about the error angular period. In this case, the error would be effectively averaged out. We plan to implement to our data acquisition algorithm such artificial drift.

Figure 8 illustrates the stability of the OSMS measurement set-up with the AC directly mounted to the carriage (Fig. 1b). In the figure, the single-scan slope error for the first and the last (8th) scans of the run measuring the first tangential trace with translation of the OSMS carriage (the run corresponds to the top plot in Fig. 6). The trace of the slope error in a particular scan was calculated as a difference of the slope distribution measured in the single scan and the distribution averaged over all eight scans of the run. Note that the scans under comparison were measured 35 hours apart.

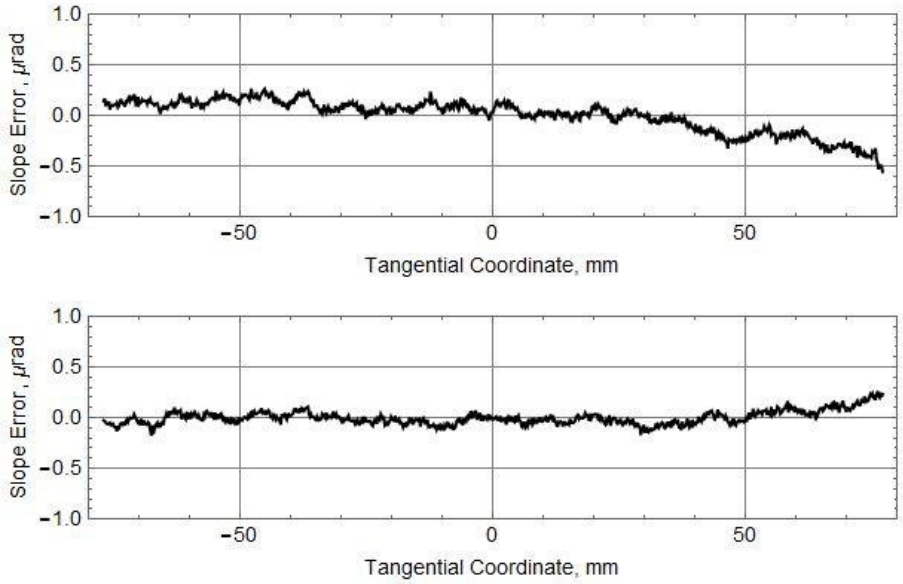

Figure 8: The measurement slope error for the 1st (the top plot) and the 8th (the bottom plot) scans of the run measuring the first tangential trace with translation of the OSMS carriage. The trace of the slope error is the difference between the slope distribution measured in a single scan and the distribution averaged over all eight scans of the run. The rms variations of the traces are 80 nrad and 64 nrad, for the top and bottom traces, respectively.

The rms variations of the slope error distributions are 80 nrad and 64 nrad, for the first and the last scans, respectively. The error distributions have a clearly seen drift error with ~0.5 μrad PV variation of opposite trends. The trends can be perfectly described with a third order polynomial function and, therefore are effectively averaged out in the result of the run consisting of 8 optimally arranged scans (see Sec. 3.1). The rest of the measurement error in a single scan (after detrending the error distributions in Fig. 8 with the best fit third polynomials) has a higher spatial frequency variation with the rms variation of 53 nrad and 43 nrad the first and the last scans, respectively.

The uncorrelated part of the higher spatial frequency variation of the single-scan error is averaged out in the resulted trace. Note that the possible contribution to the scan error of a correlated quasiperiodic component is effectively removed from the error of a single scan by subtraction of the averaged error trace.

Therefore, we can estimate the precision (repeatability) of a single run of a 2D measurement with the OSMS in the present configuration to be better than 50 nrad (rms).

5. CONCLUSION

In this article we have presented the results of comprehensive characterization of the key elements of the new Optical Surface Measuring System under development at the ALS XROL, a multifunctional translation system comprised a 2D-translation granite gantry system and a high precision tilting and flipping stage. The performed investigations have confirmed that the performance of the OSMS MFTS is totally adequate for the long term (a few days long) runs needed for 2D trace profilometry with state-of-the-art x-ray optics.

We have firstly suggested and demonstrated the extension of the optimal scanning strategy method[34] to the case of 2D surface slope measurements. The suggested measurement strategy was applied to 2D slope measurements with a high quality hyperbolic cylinder x-ray mirror. The efficiency of the developed 2D mapping have been verified via comparison

with 1D slope measurements performed with the same hyperbolic test mirror using the ALS developmental long trace profiler.

The performed investigations allow us to estimate the precision (repeatability) of a single run of a 2D measurement with the OSMS in the present configuration to be better than 50 nrad (rms). The comparison of the 2D (with the OSMS) and 1D (with the DLTP) measurements has confirmed the accuracy of the OSMS in the current simplest configuration to be on the level of 100 nm rms in the measurements with an x-ray mirror with radius of curvature of ~60 m.

Our next goals are to finalize the OSMS data acquisition and analysis software and to develop state-of-the-art optical sensors for the OSMS. The work in this directions is in progress.

ACKNOWLEDGEMENTS

J. A. is very grateful to the ALS for providing the opportunity to work in a top level scientific environment and especially to his supervisor V. V. Y. for welcoming him to the ALS, and to ENSICAEN for giving him the opportunity for the internship. The Advanced Light Source is supported by the Director, Office of Science, Office of Basic Energy Sciences, Material Science Division, of the U.S. Department of Energy under Contract No. DE-AC02- 05CH11231 at Lawrence Berkeley National Laboratory.

REFERENCES

[1] ALS-U, home page; https://als.lbl.gov/als-u/.
[2] Kevan, S., Chair, [ALS-U: Solving Scientific Challenges with Coherent Soft X-Rays], Workshop report on early science enabled by the Advanced Light Source Upgrade, ALS, LBNL, Berkeley, CA (January 18–20, 2017); https://als.lbl.gov/wp-content/uploads/2017/08/ALS-U-Early-Science-Workshop-Report-Full.pdf.
[3] Samoylova, L., Sinn, H., Siewert, F., Mimura, H., Yamauchi, K., and Tschentscher, T., "Requirements on Hard X-ray Grazing Incidence Optics for European XFEL: Analysis and Simulation of Wavefront Transformations," Proc. SPIE 7360, 73600E/1-9 (2009).
[4] Assoufid, L., and Rabedeau, T., Co-Chairs, "X-ray Mirrors," in: X-ray Optics for BES Light Source Facilities, Report of the Basic Energy Sciences Workshop on X-ray Optics for BES Light Source Facilities, D. Mills and H. Padmore, Co-Chairs, pp. 118-129, U.S. Department of Energy, Office of Science, Potomac, MD (March 27-29, 2013); http://science.energy.gov/~/media/bes/pdf/reports/files/BES_XRay_Optics_rpt.pdf.
[5] Yashchuk, V. V., Samoylova, L., and Kozhevnikov, I. V., "Specification of x-ray mirrors in terms of system performance: A new twist to an old plot," Proc. SPIE 9209, 92090F/1-19 (2014).
[6] Yashchuk, V. V., Samoylova, L., and Kozhevnikov, I. V., "Specification of x-ray mirrors in terms of system performance: A new twist to an old plot," Opt. Eng. 54(2), 025108/1-13 (2015).
[7] Cocco, D., "Recent Developments in UV Optics for Ultra-Short, Ultra-Intense Coherent Light Sources," Photonics 2015, 2(1), 40-49 (2015).
[8] Idir, M., and Yashchuk, V. V., Co-Chairs, "Optical and X-ray metrology," in: X-ray Optics for BES Light Source Facilities, Report of the Basic Energy Sciences Workshop on X-ray Optics for BES Light Source Facilities, D. Mills and H. Padmore, Co-Chairs, pp. 44-55, U.S. Department of Energy, Office of Science, Potomac, MD (March 27-29, 2013); http://science.energy.gov/~/media/bes/pdf/reports/files/BES_XRay_Optics_rpt.pdf.
[9] Yashchuk, V. V., Artemiev, N. A., Lacey, I., McKinney, W. R. and Padmore, H. A., "Advanced environmental control as a key component in the development of ultra-high accuracy ex situ metrology for x-ray optics," Opt. Eng. 54(10), 104104/1-14 (2015); doi: 10.1117/1.OE.54.10.104104.

[10] Yashchuk, V. V., Artemiev, N. A., Lacey, I., McKinney, W. R. and Padmore, H. A., "A new X-ray optics laboratory (XROL) at the ALS: Mission, arrangement, metrology capabilities, performance, and future plans," Proc. SPIE 9206, 92060I/1-19 (2014); doi:10.1117/12.2062042.
[11] Kirschman, J. L., Domning, E. E., McKinney, W. R., Morrison, G. Y., Smith, B. V., Yashchuk, V. V., "Performance of the upgraded LTP-II at the ALS optical metrology laboratory," Proc. SPIE 0770A-1 (2008).
[12] McKinney, W. R., Anders, M., Barber, S. K., Domning, E. E., Lou, Y., Morrison, G. Y., Salmassi, F., Smith, B. V., Yashchuk, V. V., "Studies in optimal configuration of the LTP", Proc. SPIE 7801, 780106-11 (2010).
[13] Yashchuk, V. V., Barber, S., Domning, E. E., Kirschman, J. L., Morrison, G. Y., Smith, B. V., Siewert, F., Zeschke, T., Geckeler, R., Just, A., "Sub-microradian surface slope metrology with the ALS developmental long trace profiler," Nucl. Instr. and Meth. A 616, 212-223 (2010).
[14] Lacey, I., Artemiev, N. A., Domning, E. E., McKinney, W. R., Morrison, G. Y., Morton, S. A., Smith, B. V., and Yashchuk, V. V., "The developmental long trace profiler (DLTP) optimized for metrology of side-facing optics at the ALS," Proc. SPIE 9206, 920603/1-11 (2014); doi:10.1117/12.2061969.
[15] Goldberg, K. A., Yashchuk, V. V., Artemiev, N. A., Celestre, R, Chao, W., Gullikson, E. M., Lacey, I., McKinney, W. R., Merthe, D., and Padmore, H. A., "Metrology for the Advancement of X-ray Optics at the ALS," Synchrotron Radiation News 26(5), 4-12, (2013); http://dx.doi.org/10.1080/08940886.2013.832583.
[16] Yashchuk, V. V., Takacs, P. Z., McKinney, W. R., Assoufid, L., Siewert, F., Zeschke, T., "Development of a new generation of optical slope measuring profiler," Nucl. Instr. and Meth. A 649(1), 153-155 (2011) - LBNL-3975E; http://doi.org/10.1016/j.nima.2010.10.063 Cited: 5 (from Web of Science).
[17] Assoufid, L., Brown, N., Crews, D., Sullivan, J., Erdmann, M., Qian, J., Jemian, P., Yashchuk, V. V., Takacs, P.Z., Artemiev, N. A., Merthe, D. J., McKinney, W. R., Siewert, F., Zeschke, T., "Development of a high-performance gantry system for a new generation of optical slope measuring profilers," Nucl. Instr. and Meth. A 710, 31-36 (2013); http://dx.doi.org/10.1016/j.nima.2012.11.063.
[18] Yashchuk, V. V., Artemiev, N. A., Centers, G. P., Chaubard, A., Geckeler, R. D., Lacey, I., Marth, H., McKinney, W. R., Noll, T., Siewert, F., Winter, M., and Zeschke, T., "High precision tilt stage as a key element to universal test mirror for characterization and calibration of slope measuring instruments," Rev. Sci. Instrum. 87(5), 051904 (2016); doi: 10.1063/1.4950729.
[19] Siewert, F., Zeschke, T., Arnold, T., Paetzold, H., and Yashchuk, V. V., "Linear chirped slope profile for spatial calibration in slope measuring deflectometry," Rev. Sci. Instrum. 87(5), 051907/1-8 (2016); doi: 10.1063/1.4950737.
[20] Geckeler, R. D., Artemiev, N. A., Barber, S. K., Just, A., Lacey, I., Kranz, O., Smith, B. V., and Yashchuk, V. V., "Aperture alignment in autocollimator-based deflectometric profilometers," Rev. Sci. Instrum. 87(5), 051906/1-8 (2016); doi: 10.1063/1.4950734.
[21] Yashchuk, V. V., Fischer, P. J., Chan, E. R., Conley, R., McKinney, W. R., Artemiev, N. A., Bouet, N., Cabrini, S., Calafiore, G., Lacey, I., Peroz, C., and Babin, S., "Binary pseudo-random patterned structures for modulation transfer function calibration and resolution characterization of a full-field transmission soft x-ray microscope," Rev. Sci. Instrum. 86(12), 123702/1-12 (2015); doi: 10.1063/1.4936752.
[22] Yashchuk, V. V., Tyurin, Yu. N., and Tyurina, A. Yu., "Modeling of surface metrology of state-of-the-art x-ray mirrors as a result of stochastic polishing process," Opt. Eng. 55(7), 074106/1-11 (2016); doi: 10.1117/1.OE.55.7.074106.
[23] Qian, J., Sullivan, J., Erdmann, M., Khounsary, A., and Assoufid, L., "Performance of the APS optical slope measuring system," Nucl. Instrum. and Meth. A 710, 48–51 (2013); https://doi.org/10.1016/j.nima.2012.10.102.
[24] Siewert, F., Noll, T., Schlegel, T., Zeschke, T., and Lammert, H., "The Nanometer Optical Component Measuring machine: a new Sub-nm Topography Measuring Device for X-ray Optics at BESSY," AIP Conference Proceedings 705, American Institute of Physics, Mellville, NY (2004), pp. 847-850.
[25] Siewert, F., Lammert, H., Zeschke, T., "The Nanometer Optical Component Measuring Machine;" in: [Modern Developments in X-Ray and Neutron Optics], Edited by A. Erko, M. Idir, T. Krist, and A. G. Michette, Springer, New York (2008).
[26] Alcock, S. G., Sawhney, K. J. S., Scott, S., Pedersen, U., Walton, R., Siewert, F., Zeschke, T., Senf, F., Noll T., and Lammert, H., "The Diamond-NOM: A non-contact profiler capable of characterizing optical figure error with sub-nanometre repeatability," Nucl. Inst. and Methods A 616(2-3), 224-228 (2010).
[27] Barber, S. K., Morrison, G. Y., Yashchuk, V. V., Gubarev, M. V., Geckeler, R. D., Buchheim, J., Siewert, F., Zeschke, T., "Developmental long trace profiler using optimally aligned mirror based pentaprism," Opt. Eng. 50(5), 053601-1-10 (2011).

[28] Barber, S. K., Geckeler, R. D., Yashchuk, V. V., Gubarev, M. V., Buchheim, J., Siewert, F., Zeschke, T., Optimal alignment of mirror based pentaprism for scanning deflectometric devices, Opt. Eng. 50(7), 0073602-1-8 (2011).
[29] Nicolas, J., Martínez, J. C., "Characterization of the error budget of Alba-NOM," Nucl. Instr. and Meth. A 710, 24-30 (2013).
[30] Qian, J., Sullivan, J., Erdmann, M., and Assoufid, L., "Performance of the APS optical slope measuring system," Nucl. Instr. and Meth. A 710, 48-51 (2013); https://doi.org/10.1016/j.nima.2012.10.102.
[31] Qian, S., Geckeler, R., Just, A., Idir, M., and Wu, H., "Approaching sub-50 nanoradian measurements by reducing the saw-tooth deviation of the autocollimator in the Nano-Optic-Measuring Machine," Nucl. Instr. and Meth. A 785, 206-212 (2015); doi: 10.1016/j.nima.2015.02.065.
[32] McKinney, W. R., and Irick, S. C., "XUV synchrotron optical components for the Advanced Light Source: Summary of the requirements and the developmental program," Proc. SPIE. 1740, 154-160 (1993); doi: 10.1117/12.138697
[33] Irick, S. C., "Error Reduction Techniques for Measuring Long Synchrotron Mirrors," Proc. SPIE 3447, 101-108 (1998); doi: 10.1117/12.331122.
[34] Yashchuk, V. V., "Optimal Measurement Strategies for Effective Suppression of Drift Errors," Rev. Sci. Instrum. 80, 115101-1-10 (2009); http://dx.doi.org/10.1063/1.3249559.
[35] Yashchuk, V. V., Artemiev, N. A., Lacey, I., and Merthe, D. J., "Correlation analysis of surface slope metrology measurements of high quality x-ray optics," Proc. SPIE 8848, 88480I-1-15 (2013); doi: 10.1117/12.2024694.
[36] Q-Sys Company website; http://www.q-sys.eu/the_company.html.
[37] OPTODYNE, Inc, [Model LDS-1000 Laser Doppler scale]; http://www.optodyne.com/opnew5/products/lds1000.pdf.
[38] Attocube, Inc., [IDS3010 integrated displacement sensing]; http://www.attocube.com/attosensorics/ids-sensors/ids3010/.
[39] Schindler, A., Haensel, T., Nickel, A., Thomas, H.-J., Lammert, H., Siewert, F., "Finishing procedure for hifh performance synchrotron Optics," Proc. SPIE 5180 (1), 70-78 (2004).
[40] Warwick, T., Anderson, C., Gaines, G., Yashchuk, V., Voronov, D., Chuang, Yi-De, and Padmore, H., "Optical and Mechanical Tolerances for QERLIN Spectrometer," LSBL Note LSBL-1279RevA (Berkeley, October, 2015).
[41] Geckeler, R., Just, A., Krause, M., Yashchuk, V. V., "Autocollimators for Deflectometry: Current Status and Future Progress," Nucl. Instr. and Meth. A 616, 140-146 (2010).
[42] McKinney, W. R. and Irick, S. C., "XUV synchrotron optical components for the Advanced Light Source: Summary of the requirements and the developmental program," Proc. SPIE. 1740, 154-160 (1993); doi: 10.1117/12.138697.